MM-wave-to-THz Modulation with Graphene-oxide-silicon Etalon Structures

W.-D. Zhang[1], **P. H. Q. Pham**[2], **E. R. Brown**[1], **and P. J. Burke**[2]

[1]Department of Physics and Electrical Engineering
Wright State University, Dayton, OH 45435, USA
[2]Department of Electrical and Computer Engineering
University of California, Irvine 92697, USA

Abstract— This paper presents both numerical modeling and experimental demonstration of a MM-wave-to-THz amplitude modulator based on a graphene-oxide-silicon etalon structure. The silicon substrate not only supports back gate bias but also acts as Fabry-Perot etalon resonant cavity for perpendicular-incident radiation. Graphene deposited on one surface of the etalon provides a tunable sheet conductance and etalon transmittance under gate bias. A 1.4-dB depth-of-modulation is measured with a 101 GHz setup, and modulation of 530 GHz radiation is also demonstrated. In all cases, the modulator behaves linearly with respect to gate bias and is easy to use because of its large aperture ($\sim$ 1 square cm) and transmission-mode operation.

1. INTRODUCTION

Millimeter-wave (MMW) and THz radiation have found application in medical imaging because their propagation characteristics can be used to sensitively detect the hydration level of targeted bio-tissues [1–3]. For the development of imaging systems, an amplitude modulator is a very useful component. The rough performance metrics of a practical modulator include $\geq$ 10 dB depth-of-modulation with at least 30 Hz of modulation bandwidth. One of the possible basis structures for a modulator is illustrated in Fig. 1(a). As a MMW-to-THz beam propagates through an etalon resonant cavity, its transmittance can be modified by a thin conducting film with tunable conductivity placed on either facet of the etalon. Of course, a conducting film also causes some absorption of the beam power.

In this paper, we report a realization of an amplitude modulator design with a graphene-oxide-silicon etalon structure [Fig. 1(b)]. The device consists of an oxide-pre-coated high-resistivity silicon substrate with a $\sim 1 \times 1$-cm monolayer-thick graphene film deposited on top. The oxide is 90 nm thick. The structure is packaged into a graphene-channel field-effect transistor (GFET) with source and drain contacts deposited on the graphene, and a (back) gate contact on the opposite side of the silicon.

For perpendicular-incident radiation, the silicon slab functions as Fabry-Perot etalon. Its transmission spectrum displays resonant peaks located at integral multiples of $f_0 = c/2nL = 112$ GHz where $L = 392\,\mu$m is the silicon thickness, and $n = 3.41$ is its refractive index [4]. The graphene sheet provides tunable conductance by the back gate bias which shifts the energy of its Fermi level.

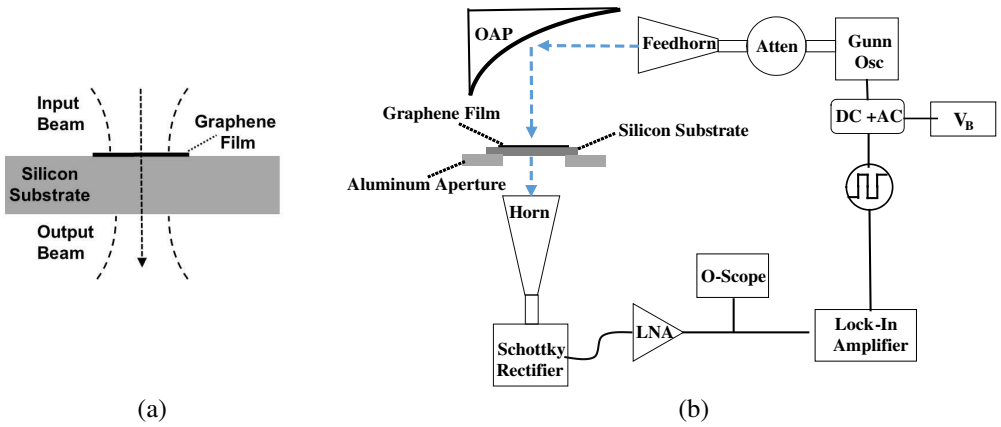

(a) (b)

Figure 1: (a) Prototype amplitude modulator (graphene-oxide-silicon etalon). (b) 101 GHz modulation setup.

Then the overall transmission of perpendicular radiation is modified proportionally. For gate tuning, graphene has already been extensively studied as optical modulators during the past several years, first in the mid-infrared [5] and then in the THz region [6–8].

2. MODELING

The transmission matrix method [9] is applied to study the effect of graphene sheet conductance on transmittance of perpendicular radiation through the graphene-oxide-silicon etalon. This yields

$$T_e = \left| \frac{t_1 t_2 \exp\left(-j\frac{2\pi\sqrt{\varepsilon_s}}{c}L\right)}{1 + r_1 r_2 \exp\left(-j\frac{4\pi\sqrt{\varepsilon_s}}{c}L\right)} \right|^2 \tag{1}$$

where r_1 is the reflection coefficient at the air/Si interface, t_1 is the transmission coefficient at the air/Si interface, r_2 is the reflection coefficient at the Si/graphene interface, and t_2 is the transmission coefficient at graphene/air interface. These parameters are linked to the dielectric constants of silicon ε_s and graphene $\varepsilon_g = \mathrm{Re}\{\varepsilon_g\} + j\mathrm{Im}\{\varepsilon_g\}$ through [10]:

$$r_1 = \frac{1-\sqrt{\varepsilon_s}}{1+\sqrt{\varepsilon_s}}, \quad t_1 = \frac{2}{1+\sqrt{\varepsilon_s}} \tag{2}$$

$$r_2 = \frac{\sqrt{\varepsilon_s} - (\sqrt{\varepsilon_g}+1)}{\sqrt{\varepsilon_s} + (\sqrt{\varepsilon_g}+1)}, \quad t_2 = \frac{2\sqrt{\varepsilon_s}}{\sqrt{\varepsilon_s} + (\sqrt{\varepsilon_g}+1)}, \tag{3}$$

The transmittance T spectra for various sheet conductances are plotted in Fig. 2(a) and confirm that the strongest modulation occurs at the resonant frequencies of the etalon located at 112, 224, 336, 448, 560 GHz, etc.. The depth-of-modulation is defined here in terms of the ratio of the high transmittance T_{high} to the low transmittance T_{low}: DoM $= 10 * \log_{10}(T_{high}/T_{low})$, all of which depend on the graphene sheet conductance at the operating frequency. As observed in Fig. 2(a), at a peak of 112 GHz, the DoM is ≈ 5.0 dB if the sheet conductance is varied from 0.66 to 5.3 mS. In contrast, at a valley frequency such as 167 GHz, the DoM drops to ~ 1.0 dB given the same variation in sheet conductance. To see the modulation effect more directly, we plot in Fig. 2(b) the transmittance vs sheet conductance for various frequencies. Here we can see that at 112 GHz the transmittance drops from 0.8 to 0.08 (DoM = 10 dB) for a change of 0.6 to 13.6 mS. And for all frequencies, greater differential T occurs at smaller values of sheet conductance, especially in the range less than 4 mS. This is associated with the fact that the resonance quality factor Q increases rapidly in this range as displayed in Fig. 2(a) [11], which does not include the imaginary part of the graphene conductance. As an example, at the sheet conductance of 0.66 mS and at the 112-GHz peak [highest-DoM case considered in Fig. 2(a)], the Q is approximately 3.5.

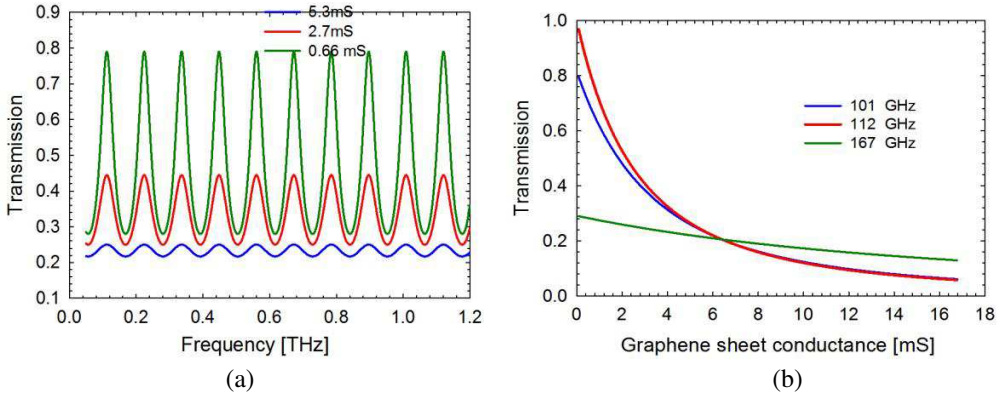

Figure 2: (a) The transmission at a sheet conductance vs. frequency. (b) The transmission at a single frequency vs. the graphene sheet conductance.

3. EXPERIMENTAL RESULTS

The graphene used in the present modulator structure was in the form of $\sim 1 \times 1$ cm films grown by CVD and then transferred from copper to silicon through a "fishing" procedure. Poly-methyl methacrylate (PMMA) was spun onto the graphene film on copper foil. The copper foil was then etched away using ammonium persulfate. Next the graphene deposited on PMMA was cleaned in DI water, and wettransferred onto a high-resistivity silicon substrate. Finally the PMMA was removed with acetone wash, and the graphene film was annealed in a hydrogen+argon atmosphere.

The first experimental setup includes a 101-GHz waveguide-mounted feedhorn-coupled Gunn-oscillator as the transmitter, and a waveguide-mounted feedhorn-coupled Schottky-rectifier as the receiver. The GFET structure was located at the focal plane of an off-axis paraboloid mirror located approximately half-way between the two [Fig. 1(b)]. The focused beam spot size is ≈ 5 mm, which is sufficiently matched to the large area of graphene. The bias to the Gunn-oscillator was square-wave amplitude modulated off-and-on with a MOSFET circuit. The detected signal from the Schottky rectifier was fed to a 1000x-gain low-noise voltage amplifier, and then demodulated with a lock-in amplifier synchronized to the square wave. The signal-to-noise ratio (SNR) was ~ 60 dB, which was determined by the average transmitted signal divided by its standard deviation over 600 sample points for the given modulation frequency (1 kHz) and lock-in amplifier integration time (0.3 ms).

The experimental results for the 101-GHz modulator are plotted in Fig. 3 where the best DoM was 1.4 dB — a 40% change. This occurred when the gate bias was varied from -4 V to $+34$ V. Simultaneously, the graphene sheet conductance (at a constant source-drain bias of 0.1 V) was monitored and changed from 1.6 mS to 0.4 mS. Beyond the gate bias of $\sim$ 33 V, however, the sheet conductance decreased no further and took an upward (V-like) turn as it hit the Dirac point. Nevertheless, the experimental DoM is reasonably close to the theoretical value, which from Fig. 2(b) is $\approx 10 * \log_{10}(0.745/0.52)$, or 1.6-dB.

Similar measurements were conducted in a higher-frequency set-up having a 530 GHz transmitter

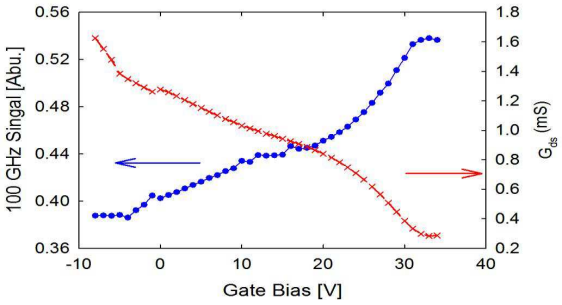

Figure 3: The measured modulation by gate bias at 101 GHz.

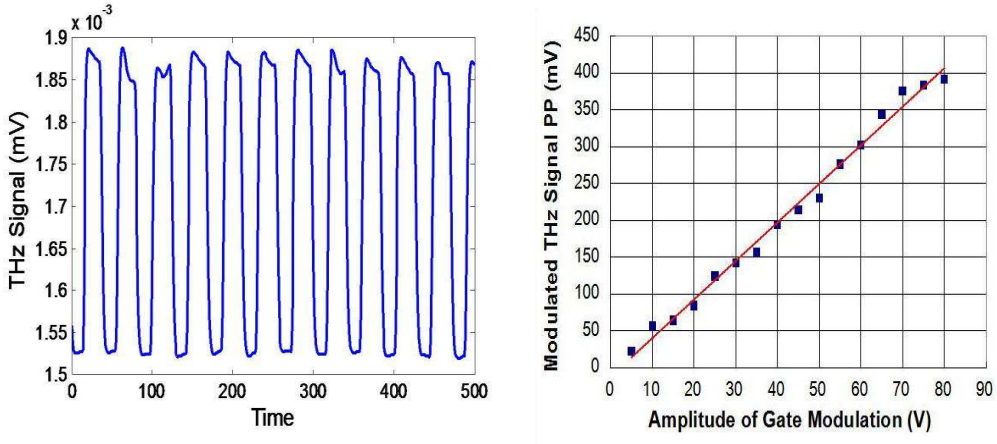

Figure 4: (a) The modulation of transmitted signal at 530 GHz. (b) The modulation amplitude as a function of gate bias.

and receiver. The transmitter consisted of a 11.0417 GHz source frequency multiplied 48x by a Schottky-diode varactor chain and coupled to free space through a diagonal feedhorn. The receiver was a low-noise Schottky-rectifier also coupled through a diagonal feedhorn and connected to a low-noise amplifier prior to lock-in demodulation. The modulation recorded with a 80 V square-wave gate bias is shown in Fig. 4(a) displaying pronounced modulation but with a DoM of only ≈ 0.8 dB. This is attributed partly to the fact that 530 GHz is 30 GHz far away from the nearest resonant peak in Fig. 2(a) at 560 GHz. Nevertheless, the modulation is still linear with gate bias as shown by the results plotted in Fig. 4(b).

4. CONCLUSIONS

We have modeled and demonstrated a voltage-controlled MMW-to-THz amplitude modulator based on a graphene-oxide-silicon etalon structure. The best measured experimental DoM was 1.4 dB at 101 GHz — less than the 10-dB goal generally applied to spatial modulators. However, analysis shows that the DoM could be enhanced by realizing greater transconductance change of the graphene film, and operating at a frequency having higher Q in the etalon. Thus there is room for improvement toward a practical MMW-to-THz amplitude modulator.

ACKNOWLEDGMENT

This material is based upon work supported by, or in part by, the U.S. Army Research Laboratory and the U.S. Army Research Office under contract number W911NF-11-1-0024.

REFERENCES

1. Gillian, C. W., B. Elizabeth, W. S. Stephen, and S. B. David, "Materials for phantoms for terahertz pulsed imaging," *Phys. Med. Biol.*, Vol. 49, N363–N369, 2004.
2. Berry, E., et al., "Optical properties of tissue measured using terahertz pulsed imaging," *Proc. SPIE*, Vol. 5030, 459–470, 2003.
3. Taylor, Z. D., et al., "Reflective terahertz imaging of porcine skin burns," *Opt. Lett.*, Vol. 33, No. 11, 1258–1260, 2008.
4. Bolivar, P. H., M. Brucherseifer, J. G. Rvivas, R. Gonzalo, I. Ederra, A. L. Reynolds, M. Holker, and P. Mgt, *IEEE Transaction on Microwave Theory and Techniques*, Vol. 51, 1062–1066, 2003.
5. Liu, M., X. Yin, E. Ulin-Avila, B. Geng, T. Zentgraf, L. Ju, F. Wang, and X. Zhang, "A graphene-based broadband optical modulator," *Nature*, Vol. 474, 64–67, 2011.
6. Sensale-Rodriguez, B., et al., "Broadband graphene terahertz modulators enabled by intraband transitions," *Nat. Commun.*, Vol. 3, 780, 2012.
7. Rahm, M., J. Li, and W. J. Padila, "THz wave modulators: A brief review on different modulation techniques," *J. Infrared Milli. Terahz Waves*, Vol. 34, 1–27, 2013.
8. Kakenov, N., et al., "Graphene-enabled electronically controlled terahertz spatial light modulator," *Opticas Letters*, Vol. 40, 1984–1987, 2015.
9. Born, M. and E. Wolf, *Principles of Optics: Electromagnetic Theory of Propagation, Interference and Diffraction of Light*, Cambridge University Press, 1993.
10. Falkovsky, L. A., *Physics-Uspekhi*, Vol. 51, 887–897, 2008.
11. We define Q in the usual way as $f_0/\Delta f_0$ where f_0 is the peak center frequency and Δf is its FWHM.